Theory of current-driven instability experiments in magnetic Taylor-Couette flows

Günther Rüdiger* and Manfred Schultz†
Astrophysikalisches Institut Potsdam, An der Sternwarte 16, D-14482 Potsdam, Germany

Dima Shalybkov‡
A.F. Ioffe Institute for Physics and Technology, 194021, St. Petersburg, Russia

Rainer Hollerbach§
Department of Applied Mathematics, University of Leeds, Leeds, LS2 9JT, United Kingdom
(Received 15 November 2006; revised manuscript received 11 June 2007; published 14 November 2007)

We consider the linear stability of dissipative magnetic Taylor-Couette flow with imposed toroidal magnetic fields. The inner and outer cylinders can be either insulating or conducting; the inner one rotates, the outer one is stationary. The magnetic Prandtl number can be as small as 10^{-5}, approaching realistic liquid-metal values. The magnetic field destabilizes the flow, except for radial profiles of $B_\phi(R)$ close to the current-free solution. The profile with $B_{\rm in}=B_{\rm out}$ (the most uniform field) is considered in detail. For weak fields the Taylor-Couette flow is *stabilized*, until for moderately strong fields the $m=1$ azimuthal mode dramatically destabilizes the flow again so that a maximum value for the critical Reynolds number exists. For sufficiently strong fields (as measured by the Hartmann number) the toroidal field is always unstable, even for the nonrotating case with Re=0. The electric currents needed to generate the required toroidal fields in laboratory experiments are a few kA if liquid sodium is used, somewhat more if gallium is used. Weaker currents are needed for wider gaps, so a wide-gap apparatus could succeed even with gallium. The critical Reynolds numbers are only somewhat larger than the nonmagnetic values; hence such experiments would work with only modest rotation rates.

DOI: 10.1103/PhysRevE.76.056309 PACS number(s): 47.20.Ft, 47.65.−d, 47.63.mf

I. MOTIVATION

Taylor-Couette flows between rotating concentric cylinders are among the fundamental problems in classical hydrodynamic stability theory, with an enormous range of possible flow states and transitions between different states. The magnetohydrodynamic analog of this problem, in which the fluid is electrically conducting and a magnetic field is externally applied, is equally important in hydromagnetic stability theory [1]. The earliest experiments on this magnetohydrodynamic problem were by Donnelly *et al.* [2,3] in the early 1960s, and focused on the inhibition of Taylor vortices by the application of increasingly strong magnetic fields. Despite the rather good agreement between the experimental results and Chandrasekhar's [1] theoretical predictions (see also [4] for more recent numerical work), the subject attracted relatively little further attention, most likely due to the difficulties of doing experiments with liquid metals.

Another intriguing aspect of magnetohydrodynamic Taylor-Couette flows is the so-called magnetorotational instability (MRI), first discovered by Velikhov in 1959 [5]. What makes the MRI particularly interesting is that the magnetic field now has a *destabilizing* effect, exactly the opposite of the stabilizing effect that it had in Donnelly's experiments. The difference is that Donnelly was operating to the left of the so-called Rayleigh line, where the flow may be destabilized purely hydrodynamically, and the addition of a magnetic field then has a stabilizing influence, whereas Velikhov was considering flows to the right of the Rayleigh line, where the flow is hydrodynamically stable, and the addition of a magnetic field may have a destabilizing influence.

However, despite its undeniable charm as a new type of hydromagnetic instability, for many decades the MRI also attracted very little further attention. It was only with the realization that it was likely to be of considerable importance in astrophysical fluid dynamics [6] that interest revived, and experimentalists started thinking about studying it in the laboratory. The original designs [7,8] called for a purely axial magnetic field, which requires very large rotation rates though, due to the extremely small magnetic Prandtl numbers of liquid metals. Instead, Hollerbach and Rüdiger [9] suggested adding an azimuthal field, which turns out to reduce the required rotation rates by several orders of magnitude. This new design has been implemented experimentally [10–12], and does indeed yield traveling-wave disturbances in agreement with the theoretical predictions [9].

The azimuthal field required to obtain this traveling-wave MRI was generated by an electric current, up to 8 kA, flowing along a copper rod running down the central axis, inside the inner cylinder. Within the fluid the field is therefore current-free, $B_\phi \propto 1/R$. In this work, we wish to consider how the situation is altered if instead the current is allowed to flow directly through the fluid as well. This allows for fundamentally new instabilities, namely so-called current-driven or Vandakurov-Tayler instabilities [13,14]. Because the source of energy is now the current rather than the differential rotation, these (nonaxisymmetric) instabilities can exist even without any differential rotation at all (very much unlike the MRI), provided only the current is sufficiently large.

*gruediger@aip.de
†mschultz@aip.de
‡dasha@astro.ioffe.ru
§rh@maths.leeds.ac.uk

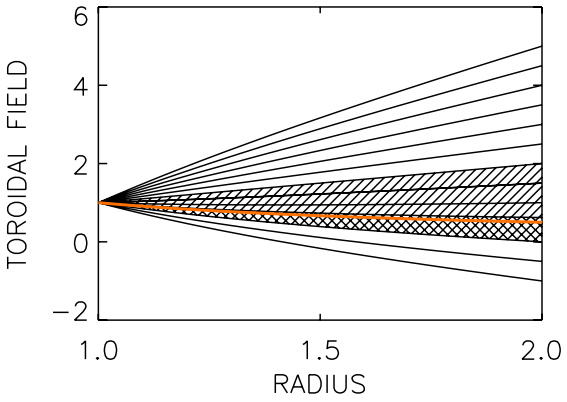

FIG. 1. (Color online) The basic state profiles of $B_\phi(R)$, for $\hat{\eta}=0.5$. Remembering that $B_\phi(1)$ has been normalized to 1, we find that $\hat{\mu}_B$ is given simply by $B_\phi(2)$, and can therefore be read off the right-hand axis. The stability domain for $m=1$ [see Eq. (21)] is cross-hatched; the cross-hatched and hatched domains together are the stability domain for $m=0$ [see Eq. (22)]. The current-free solution $B_\phi=1/R$ is given by the gray line ($\hat{\mu}_B=0.5$). The electric currents inside and outside the inner cylinder are parallel above $\hat{\mu}_B=0.5$ and antiparallel below $\hat{\mu}_B=0.5$; that is, the signs of a_B and b_B are the same above 0.5, and opposite below.

The main point we wish to demonstrate in this work is that currents no greater than the 8 kA already used in the MRI experiments [10–12] are sufficient to generate current-driven instabilities as well. We therefore present a detailed series of numerical calculations outlining the optimal design for obtaining current-driven instabilities in Taylor-Couette experiments.

Finally, although in this work we will focus exclusively on the details of a possible laboratory experiment, we note briefly that the combination of current-driven instabilities and differential rotation may also be relevant to a broad range of astrophysical problems, including the stability of the solar tachocline, the existence of active solar longitudes [15], the flip-flop phenomenon of stellar activity [16], A-star magnetism [17], and dynamo action in stably stratified stars [18].

II. EQUATIONS

According to the Rayleigh criterion, an ideal flow is stable against axisymmetric perturbations whenever the specific angular momentum increases outwards

$$\frac{d}{dR}(R^2\Omega)^2 > 0, \tag{1}$$

where $(R,\ \phi,\ z)$ are cylindrical coordinates and Ω is the angular velocity. The necessary and sufficient condition for the axisymmetric stability of an ideal Taylor-Couette flow with an imposed azimuthal magnetic field B_ϕ is

$$\frac{1}{R^3}\frac{d}{dR}(R^2\Omega)^2 - \frac{R}{\mu_0\rho}\frac{d}{dR}\left(\frac{B_\phi}{R}\right)^2 > 0, \tag{2}$$

where μ_0 is the permeability and ρ the density [1,19]. In particular, *all* ideal flows can thus be destabilized, by azimuthal magnetic fields with the right profiles and amplitudes. Any fields increasing outward more slowly than $B_\phi \propto R$, including in particular the outwardly decreasing current-free field $B_\phi \propto 1/R$, have a stabilizing influence though [5].

Tayler [14] found the necessary and sufficient condition

$$-\frac{d}{dR}(RB_\phi^2) > 0 \tag{3}$$

for the nonaxisymmetric stability of an ideal fluid at rest. Outwardly increasing fields are therefore unstable now (but $B_\phi \propto 1/R$ is still stable). If this condition (3) is violated, the most unstable mode has azimuthal wave number $m=1$. In this paper, we wish to consider how these Tayler instabilities are modified if the fluid is not at rest, but is instead differentially rotating.

We will find that, depending on the magnitudes of the imposed differential rotation and magnetic fields, and also on the magnetic Prandtl number, a magnetic field may either stabilize or destabilize the differential rotation, and the most unstable mode may be either the axisymmetric Taylor vortex flow, or the nonaxisymmetric Tayler instability. We focus on the limit of small magnetic Prandtl numbers appropriate for liquid metals, and calculate the rotation rates and electric currents that would be required to obtain some of these instabilities in liquid metal laboratory experiments.

The governing equations are

$$\frac{\partial \mathbf{U}}{\partial t} + (\mathbf{U}\nabla)\mathbf{U} = -\frac{1}{\rho}\nabla P + \nu\Delta\mathbf{U} + \frac{1}{\mu_0}\mathrm{curl}\ \mathbf{B}\times\mathbf{B}, \tag{4}$$

$$\frac{\partial \mathbf{B}}{\partial t} = \mathrm{curl}(\mathbf{U}\times\mathbf{B}) + \eta\Delta\mathbf{B}, \tag{5}$$

and

$$\mathrm{div}\ \mathbf{U} = \mathrm{div}\ \mathbf{B} = 0, \tag{6}$$

where $\mathbf{U}$ is the velocity, $\mathbf{B}$ the magnetic field, P the pressure, ν the kinematic viscosity, and η the magnetic diffusivity.

The basic state is $U_R=U_z=B_R=B_z=0$ and

$$U_\phi = R\Omega = a_\Omega R + \frac{b_\Omega}{R}, \quad B_\phi = a_B R + \frac{b_B}{R}, \tag{7}$$

where a_Ω, b_Ω, a_B, and b_B are constants defined by

$$a_\Omega = \Omega_{\mathrm{in}}\frac{\hat{\mu}_\Omega - \hat{\eta}^2}{1-\hat{\eta}^2}, \quad b_\Omega = \Omega_{\mathrm{in}}R_{\mathrm{in}}^2\frac{1-\hat{\mu}_\Omega}{1-\hat{\eta}^2},$$

$$a_B = \frac{B_{\mathrm{in}}}{R_{\mathrm{in}}}\frac{\hat{\eta}(\hat{\mu}_B - \hat{\eta})}{1-\hat{\eta}^2}, \quad b_B = B_{\mathrm{in}}R_{\mathrm{in}}\frac{1-\hat{\mu}_B\hat{\eta}}{1-\hat{\eta}^2}, \tag{8}$$

where

$$\hat{\eta} = \frac{R_{\mathrm{in}}}{R_{\mathrm{out}}}, \quad \hat{\mu}_\Omega = \frac{\Omega_{\mathrm{out}}}{\Omega_{\mathrm{in}}}, \quad \hat{\mu}_B = \frac{B_{\mathrm{out}}}{B_{\mathrm{in}}}. \tag{9}$$

R_{in} and R_{out} are the radii of the inner and outer cylinders, Ω_{in} and Ω_{out} are their rotation rates (we will in fact fix $\Omega_{\mathrm{out}}=0$ for all results presented here), and B_{in} and B_{out} are the azimuthal magnetic fields at the inner and outer cylinders. The

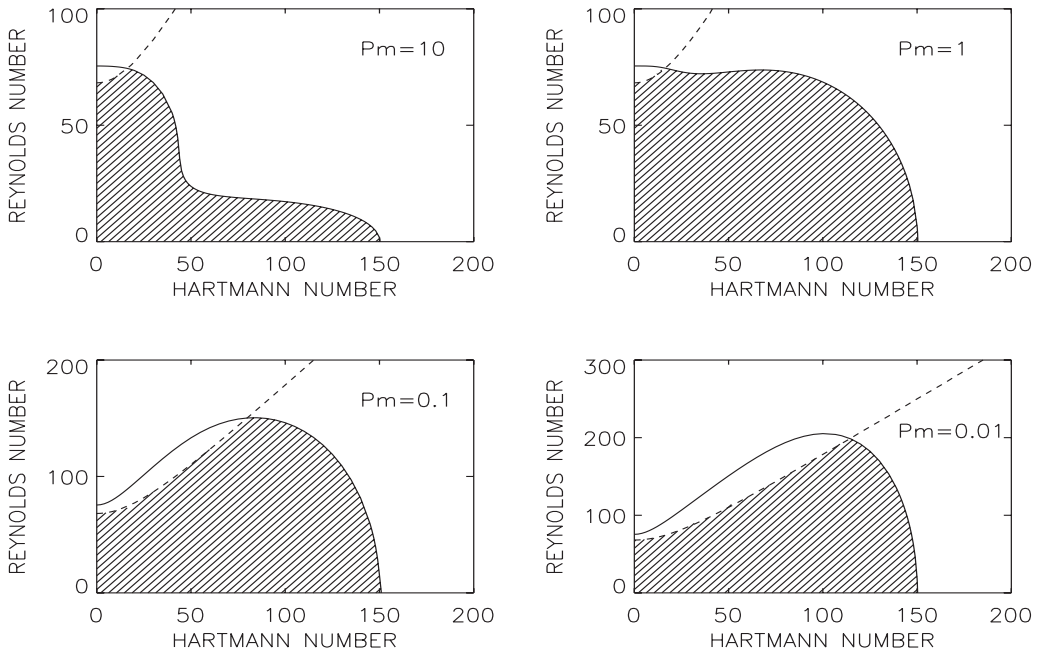

FIG. 2. Marginal stability curves for $m=0$ (dashed) and $m=1$ (solid). The hatched area is thus the region that is stable to both. Magnetic Prandtl numbers as indicated on each plot.

possible magnetic field solutions are plotted in Fig. 1. Note though that—unlike Ω, where Ω_{in} and Ω_{out} are the physically relevant quantities—for B_ϕ the fundamental quantities are not so much B_{in} and B_{out}, but rather a_B and b_B themselves. In particular, a field of the form b_B/R is generated by running an axial current only through the inner region $R<R_{\text{in}}$, whereas a field of the form $a_B R$ is generated by running an axial current through the entire region $R<R_{\text{out}}$, including the fluid. One of the aspects we will be interested in later on is how large these currents must be, and whether they could be generated in a laboratory experiment.

We are interested in the linear stability of the basic state (7). The perturbed quantities of the system are given by

$$u_R,\ R\Omega + u_\phi,\ u_z,\ b_R,\ B_\phi + b_\phi,\ b_z. \tag{10}$$

Applying the usual normal mode analysis, we look for solutions of the linearized equations of the form

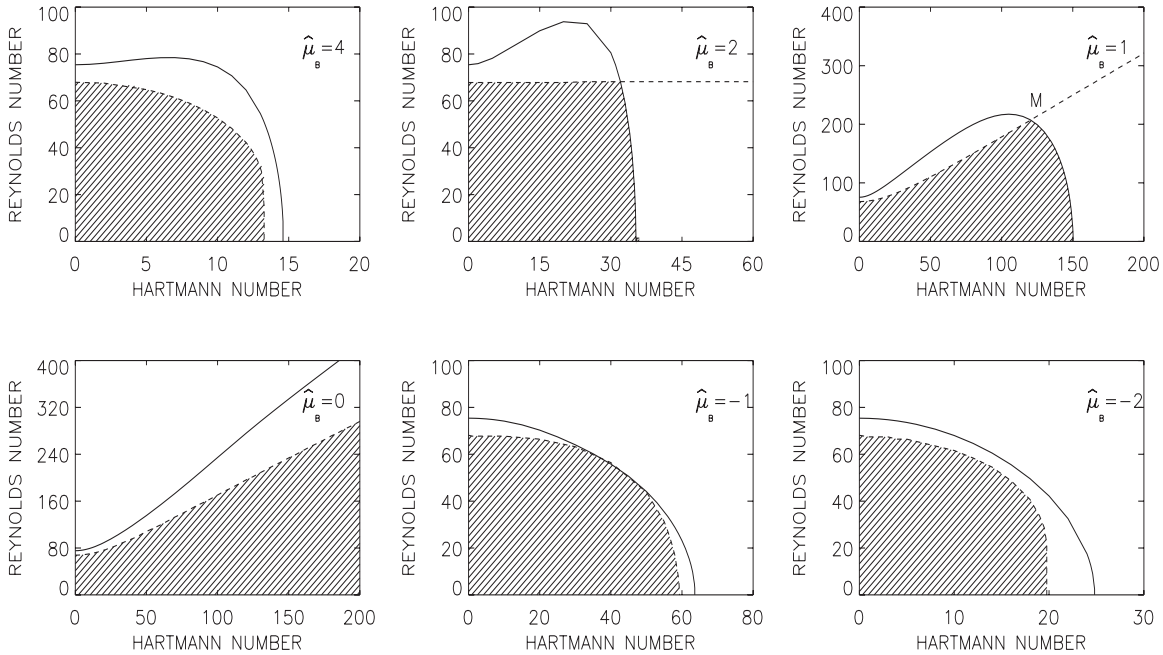

FIG. 3. The marginal stability curves for $m=0$ (dashed) and $m=1$ (solid). $\text{Pm}=10^{-5}$, $\hat{\eta}=0.5$, $\hat{\mu}_\Omega=0$, and $\hat{\mu}_B$ as indicated. Note also how the critical Reynolds numbers are always of the same order of magnitude as the nonmagnetic result 68, which is easy to achieve in the laboratory.

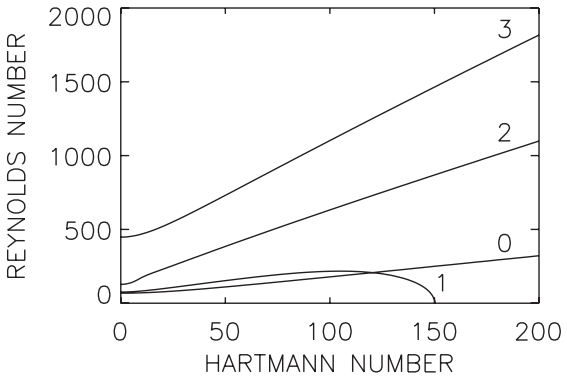

FIG. 4. The instability lines for $\hat{\mu}_B=1$ (shown in Fig. 3, top right) for various m. Note that only the $m=1$ mode exhibits the Tayler instability.

$$F = F(R)\exp[i(kz + m\phi + \omega t)]. \tag{11}$$

The dimensionless numbers of the problem are the magnetic Prandtl number Pm, the Hartmann number Ha, and the Reynolds number Re, given by

$$\mathrm{Pm} = \frac{\nu}{\eta}, \quad \mathrm{Ha} = \frac{B_{\mathrm{in}} R_0}{\sqrt{\mu_0 \rho \nu \eta}}, \quad \mathrm{Re} = \frac{\Omega_{\mathrm{in}} R_0^2}{\nu}, \tag{12}$$

where $R_0=[R_{\mathrm{in}}(R_{\mathrm{out}}-R_{\mathrm{in}})]^{1/2}$ is the unit of length.

Using Eq. (11), linearizing Eqs. (4) and (5), and representing the result as a system of first order equations, we have

$$\frac{du_R}{dR} + \frac{u_R}{R} + i\frac{m}{R}u_\phi + iku_z = 0,$$

$$\frac{dP}{dR} + i\frac{m}{R}X_2 + ikX_3 + \left(k^2 + \frac{m^2}{R^2}\right)u_R + i\,\mathrm{Re}(\omega + m\Omega)u_R - 2\Omega\,\mathrm{Re}\,u_\phi - i\,\mathrm{Ha}^2\frac{m}{R}B_\phi b_R + 2\,\mathrm{Ha}^2\frac{B_\phi}{R}b_\phi = 0,$$

$$\frac{dX_2}{dR} - \left(k^2 + \frac{m^2}{R^2}\right)u_\phi - i\,\mathrm{Re}(\omega + m\Omega)u_\phi + 2i\frac{m}{R^2}u_R - \frac{\mathrm{Re}}{R}\frac{d}{dR}(R^2\Omega)u_R + \frac{\mathrm{Ha}^2}{R}\frac{d}{dR}(RB_\phi)b_R + i\,\mathrm{Ha}^2\frac{m}{R}B_\phi b_\phi - i\frac{m}{R}P = 0,$$

$$\frac{dX_3}{dR} + \frac{X_3}{R} - \left(k^2 + \frac{m^2}{R^2}\right)u_z - i\,\mathrm{Re}(\omega + m\Omega)u_z - ikP + i\,\mathrm{Ha}^2\frac{m}{R}B_\phi b_z = 0,$$

$$\frac{db_R}{dR} + \frac{b_R}{R} + i\frac{m}{R}b_\phi + ikb_z = 0,$$

$$\frac{db_z}{dR} - \frac{i}{k}\left(k^2 + \frac{m^2}{R^2}\right)b_R + \mathrm{Pm}\,\mathrm{Re}\frac{1}{k}(\omega + m\Omega)b_R + \frac{1}{k}\frac{m}{R}X_4 - \frac{1}{k}\frac{m}{R}B_\phi u_R = 0,$$

$$\frac{dX_4}{dR} - \left(k^2 + \frac{m^2}{R^2}\right)b_\phi - i\,\mathrm{Pm}\,\mathrm{Re}(\omega + m\Omega)b_\phi + i\frac{2m}{R^2}b_R - R\frac{d}{dR}\left(\frac{B_\phi}{R}\right)u_R + \mathrm{Pm}\,\mathrm{Re}\,R\frac{d\Omega}{dR}b_r + i\frac{m}{R}B_\phi u_\phi = 0, \tag{13}$$

where X_2, X_3, and X_4 are defined as

$$X_2 = \frac{du_\phi}{dR} + \frac{u_\phi}{R}, \quad X_3 = \frac{du_z}{dR}, \quad X_4 = \frac{db_\phi}{dR} + \frac{b_\phi}{R}. \tag{14}$$

Length has been scaled by R_0, time by $\Omega_{\mathrm{in}}^{-1}$, the basic state angular velocity by Ω_{in}, the perturbation velocity by η/R_0, and the magnetic fields, both basic state and perturbation, by B_{in}.

An appropriate set of ten boundary conditions is needed to solve the system (13). For the velocity the boundary conditions are always no-slip,

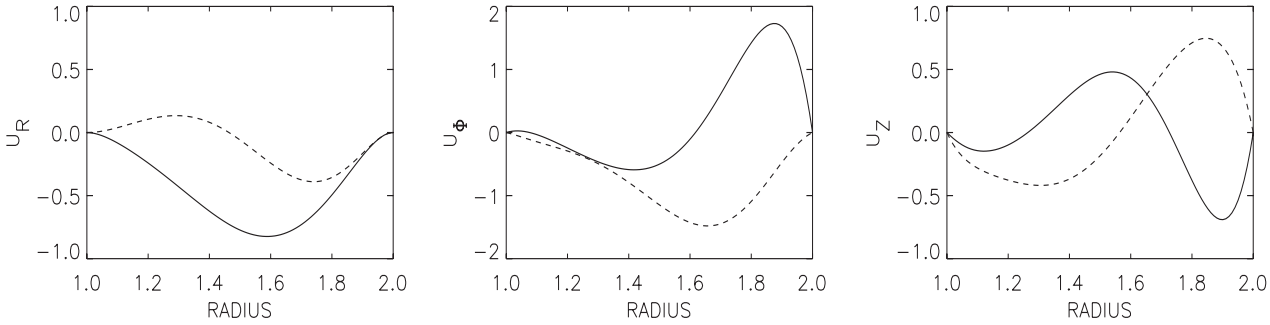

FIG. 5. The flow pattern ($m=1$) for a container with conducting walls and a fluid with $\mathrm{Pm}=10^{-5}$. The parameters are $\mathrm{Ha}=120$ and $\mathrm{Re}=208$ describing the location of the intersection M in Fig. 3 (top right). The radial profiles of u_R (left), u_ϕ (middle), and u_z (right) are shown. Solid (dashed): Real (imaginary) part of the solution.

TABLE I. Material parameters of liquid metals that might be used for magnetic TC experiments.

	ρ (g/cm^3)	ν (cm^2/s)	η (cm^2/s)
Sodium	0.92	7.10×10^{-3}	0.81×10^{3}
Gallium-indium-tin	6.36	3.40×10^{-3}	2.43×10^{3}

$$u_R = u_\phi = u_z = 0. \tag{15}$$

For the magnetic field the boundary conditions depend on whether the walls are insulators or conductors. For conducting walls the radial component of the field and the tangential components of the current must vanish, yielding

$$db_\phi/dR + b_\phi/R = b_R = 0. \tag{16}$$

These boundary conditions are applied at both R_{in} and R_{out}.

For insulating walls the boundary conditions are somewhat more complicated; matching to interior and exterior potential fields then yields

$$b_\phi = \frac{m}{kR} b_z, \tag{17}$$

$$b_R + \frac{ib_z}{I_m(kR)}\left(\frac{m}{kR} I_m(kR) + I_{m+1}(kR)\right) = 0, \tag{18}$$

at $R=R_{\text{in}}$, and

$$b_\phi = \frac{m}{kR} b_z, \tag{19}$$

$$b_R + \frac{ib_z}{K_m(kR)}\left(\frac{m}{kR} K_m(kR) - K_{m+1}(kR)\right) = 0 \tag{20}$$

at $R=R_{\text{out}}$, where I_n and K_n are the modified Bessel functions [20].

TABLE II. Characteristic Hartmann numbers and electric currents for a wide gap container ($\hat{\eta}=0.25$) with conducting walls, using either sodium or gallium-indium-tin (in brackets).

$\hat{\mu}_B$	Ha$^{(0)}$	Ha$^{(1)}$	I_{axis} (kA)	I_{fluid} (kA)
−10	2.29	2.05	0.0483 (0.152)	−1.98 (−6.24)
−5	4.23	3.98	0.0937 (0.296)	−1.97 (−6.21)
−4	5.14	4.93	0.116 (0.366)	−1.97 (−6.22)
−3	6.63	6.50	0.153 (0.483)	−1.99 (−6.27)
−2	9.69	9.71	0.228 (0.721)	−2.05 (−6.49)
−1	24.7	22.5	0.530 (1.67)	−2.65 (−8.35)
1	**∞**	**41.7**	**0.982 (3.10)**	**2.94 (9.29)**
2	∞	13.8	0.325 (1.02)	2.27 (7.17)
3	∞	8.27	0.195 (0.614)	2.14 (6.75)
4	∞	5.93	0.140 (0.440)	2.09 (6.60)
5	10.8	4.63	0.109 (0.344)	2.07 (6.53)
10	3.23	2.205	0.0519 (0.164)	2.02 (6.39)

TABLE III. As in Table II, but for $\hat{\eta}=0.5$, and conducting boundaries.

$\hat{\mu}_B$	Ha$^{(0)}$	Ha$^{(1)}$	I_{axis} (kA)	I_{fluid} (kA)
−10	3.96	5.02	0.161 (0.509)	−3.39 (−10.7)
−5	7.73	9.85	0.315 (0.994)	−3.47 (−10.9)
−4	9.61	12	0.392 (1.24)	−3.53 (−11.1)
−3	12.8	16.2	0.522 (1.65)	−3.65 (−11.5)
−2	19.8	24.8	0.807 (2.55)	−4.04 (−12.7)
−1	59.3	63.7	2.42 (7.63)	−7.25 (−22.9)
1	**∞**	**151**	**6.16 (19.4)**	**6.16 (19.4)**
2	∞	35.3	1.44 (4.54)	4.32 (13.6)
3	21.0	20.6	0.840 (2.65)	4.20 (13.2)
4	13.2	14.6	0.538 (1.70)	3.77 (11.9)
5	9.84	11.4	0.401 (1.27)	3.61 (11.4)
10	4.44	5.4	0.181 (0.571)	3.44 (10.8)

Given the basic state (7), Tayler's stability condition (3) to nonaxisymmetric perturbations becomes

$$0 < \hat{\mu}_B < \frac{4\hat{\eta}(1-\hat{\eta}^2)}{3-2\hat{\eta}^2-\hat{\eta}^4} \equiv \hat{\mu}_1. \tag{21}$$

Note that $\hat{\mu}_1 \to 1$ (but is always less than 1) if $\hat{\eta}\to 1$. For $\hat{\eta}=0.5$ we have $\hat{\mu}_1=0.62$. Similarly, the stability condition to axisymmetric perturbations becomes

$$0 < \hat{\mu}_B < \frac{1}{\hat{\eta}} \equiv \hat{\mu}_0. \tag{22}$$

For $\hat{\eta}=0.5$ we have $\hat{\mu}_0=2$. For $0<\hat{\eta}<1$ we always have $\hat{\mu}_1<\hat{\mu}_0$, so that the stability interval (21) for $m=1$ is much smaller than the stability interval (22) for $m=0$, as shown in Fig. 1. The current-free solution $\hat{\mu}_B=0.5$ is of course always stable.

III. BASIC RESULTS

Figure 2 shows how the stability curves depend on Ha and Re, for Pm=10, 1, 0.1, and 0.01, with $\hat{\mu}_\Omega=0$ (stationary outer cylinder) and $\hat{\mu}_B=1$ (B_ϕ as uniform as possible). For Ha=0 we find that $m=0$ goes unstable before $m=1$, at the critical Reynolds number $\text{Re}_{\text{crit}}=68$; this is just the familiar value for the onset of nonmagnetic Taylor vortices (at this particular radius ratio). Being entirely nonmagnetic, this value obviously does not depend on Pm. At the other limiting case, Re=0, we find that only $m=1$ goes unstable, at the critical Hartmann number $\text{Ha}_{\text{crit}}=150$. These Tayler instabilities also turn out to be independent of Pm, despite being driven by the magnetic field.

We are interested in how these two limiting cases Ha=0 and Re=0 are connected, and how the two types of instabilities interact when neither parameter is zero. The two instabilities certainly are connected; the $m=1$ modes in the two limiting cases are smoothly joined to one another for all Prandtl numbers. The nature of the interaction is quite different though, depending on Pm.

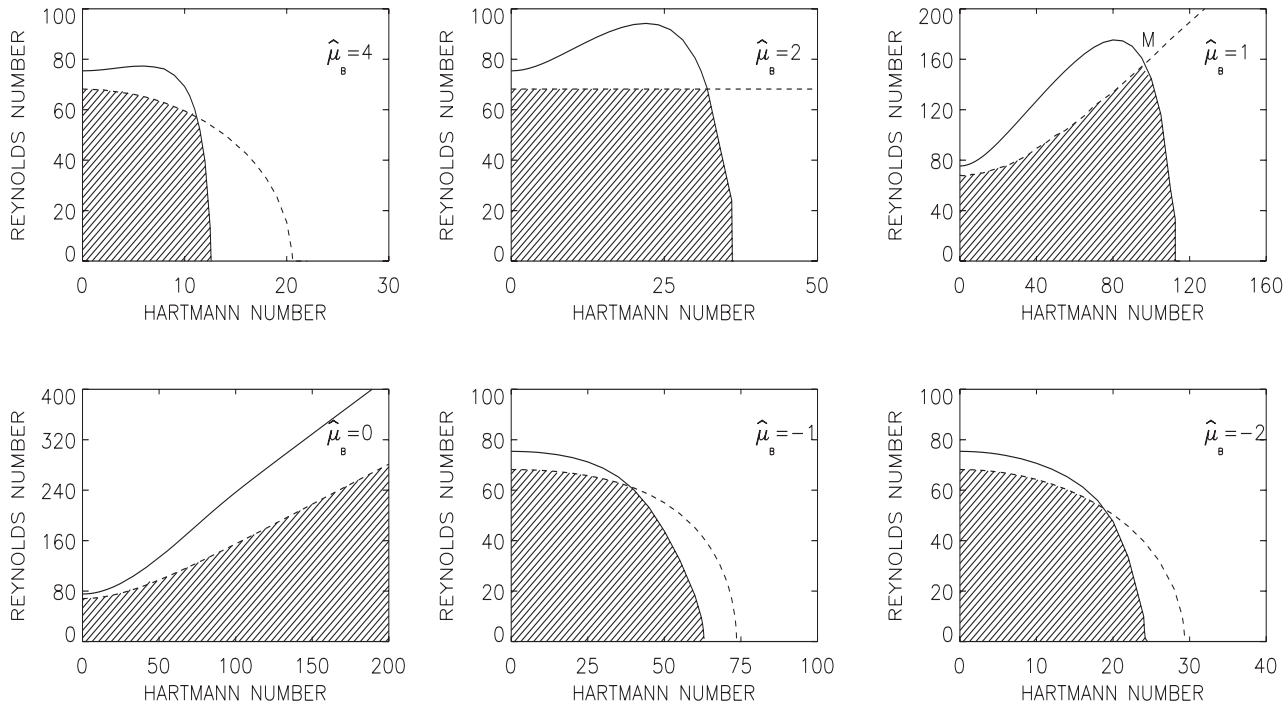

FIG. 6. The same as in Fig. 3 but for insulating cylinder walls.

Turning to Pm=1 first, we see that there is relatively little interaction between rotational and magnetic effects; instability simply sets in as long as either $\mathrm{Ha} > \mathrm{Ha}_{\mathrm{crit}}$ or $\mathrm{Re} > \mathrm{Re}_{\mathrm{crit}}$. For Pm=10 the situation is very different. There we find a broad range of parameters, for example, Ha=100 and Re =50, that would be stable if rotational or magnetic effects were acting alone, but which are now unstable, due to the interaction between the two (see also [21]). Finally, for Pm =0.1 we have the opposite situation, namely a range of parameters, for example, Ha=100 and Re=100, that would be unstable if rotational effects were acting alone, but which are now stable.

Small Pm are generally stabilizing. The opposite is true for Pm>1. As shown in Fig. 2 (top left), instability then also sets in for Hartmann numbers less than 150. In other words, for Hartmann numbers exceeding around 50, the critical Reynolds number for the onset of instability is much smaller than 68.

IV. LIQUID METALS

Having explored the general behavior for a range of magnetic Prandtl numbers, we now focus attention on the limit of very small Pm, such as would apply for experiments involving liquid metals. We will here consider conducting and insulating boundary conditions separately.

A. Conducting cylinder walls

Figure 3 shows results for various values of $\hat{\mu}_B$; a_B and b_B are the same sign for the values in the top row, and the opposite sign for the values in the bottom row. The profile that is closest to being current-free is $\hat{\mu}_B=0$, and indeed we find there that even for Ha=200 there is no sign of any destabilizing influence of the field, for either axisymmetric or nonaxisymmetric perturbations. For $0<\hat{\mu}_B<\hat{\mu}_1$ the magnetic field stabilizes the flow for both $m=0$ and $m=1$.

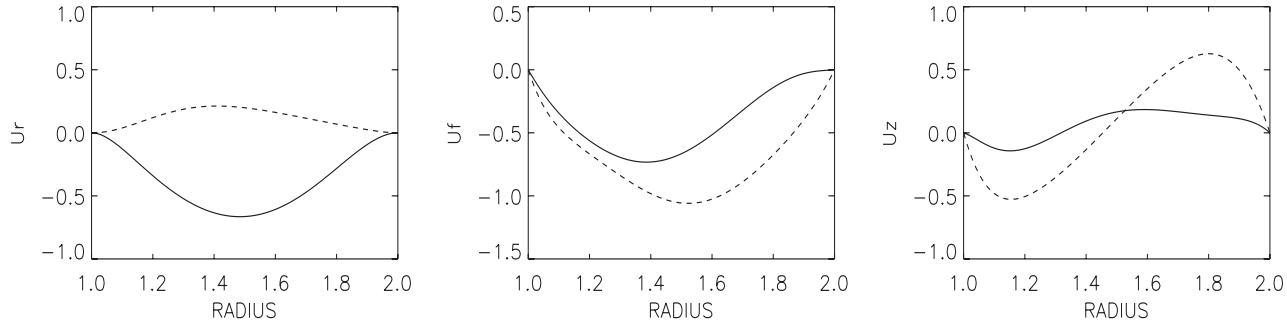

FIG. 7. The same as in Fig. 5 but for insulating cylinder walls. At the intersection point M the wave number is $k=3.56$, so the vertical structure is again comparable to the gap width.

TABLE IV. As in Table II, but for $\hat{\eta}=0.25$, and insulating boundaries.

$\hat{\mu}_B$	Ha_0	Ha_1	I_{axis} (kA)	I_{fluid} (kA)
−10	3.63	1.79	0.0421 (0.133)	−1.73 (−5.45)
−5	6.65	3.55	0.0836 (0.264)	−1.76 (−5.54)
−4	8.04	4.42	0.104 (0.328)	−1.77 (−5.58)
−3	10.3	5.89	0.139 (0.437)	−1.81 (−5.68)
−2	14.7	8.91	0.210 (0.662)	−1.89 (−5.60)
−1	30.6	20.5	0.483 (1.52)	−2.42 (−7.60)
1	**∞**	**30.7**	**0.723 (2.28)**	**2.17 (6.84)**
2	∞	10.7	0.252 (0.794)	1.76 (5.56)
3	∞	6.63	0.156 (0.492)	1.72 (5.41)
4	∞	4.83	0.114 (0.359)	1.71 (5.39)
5	17.4	3.81	0.0897 (0.283)	1.70 (5.38)
10	5.18	1.86	0.0438 (0.138)	1.71 (5.38)

For $\hat{\mu}_1<\hat{\mu}_B<\hat{\mu}_0$ the $m=1$ mode should be unstable, while the $m=0$ mode should be stable. The values $\hat{\mu}_B=1$ and $\hat{\mu}_B=2$ are examples of this situation. There is always a crossover point at which the most unstable mode changes from $m=0$ to $m=1$. Note also how for $\hat{\mu}_B=1$, the critical Reynolds number increases for the $m=0$ mode, before suddenly decreasing for the $m=1$ mode (Fig. 3, top right). We have the interesting situation therefore that weak fields initially stabilize the TC flow, before stronger fields eventually destabilize it, via a nonaxisymmetric mode. Beyond Ha=150 (the same value we saw previously in Fig. 2), the flow is unstable even for Re=0.

Except for the almost current-free profile $\hat{\mu}_B=0$, all other values share this feature, that there is a critical Hartmann number beyond which the basic state is unstable even for Re=0. Let $\mathrm{Ha}^{(0)}$ and $\mathrm{Ha}^{(1)}$ denote these critical Hartmann numbers, for $m=0$ and 1, respectively. For the profiles with the largest gradients both modes are unstable. Strikingly, in these cases $m=0$ is always more unstable than $m=1$, that is, $\mathrm{Ha}^{(0)}<\mathrm{Ha}^{(1)}$; see the plots for $\hat{\mu}_B=4$ and $\hat{\mu}_B=-2$ of Fig. 3.

The standard case with $\hat{\mu}_B=1$ (shown in Fig. 3, top right) has been considered in more detail. In Fig. 4 the stability lines for disturbances of higher m are plotted. Note the exceptional role of the mode with $m=1$, as the only one that cannot be stabilized by the differential rotation if the Hartmann number exceeds the threshold value. All the modes other than $m=1$ are stabilized by the magnetic field.

For the same experiment the flow pattern for $m=1$ at the intersection M of the modes $m=0$ and $m=1$ is represented in Fig. 5. There are several cells in radius, but one cannot find striking anisotropies. The vertical wave number is $k=4.58$ so that from the relation

$$\frac{\delta z}{R_{\mathrm{out}}-R_{\mathrm{in}}}=\frac{\pi}{k}\sqrt{\frac{\hat{\eta}}{1-\hat{\eta}}}, \tag{23}$$

the vertical extension of a cell is only 68% of the gap width (here $\hat{\eta}=0.5$). Hence the cells are rather flat and we shall have not too many problems with the end plates of a real container. As a nonaxisymmetric instability there is a finite value of the azimuthal drift of the flow pattern. One can also describe it as a (nonaxisymmetric) vertical wave. The azimuthal drift rate is −0.34, in units of the rotation rate of the inner cylinder. At the intersection of the curve for $m=1$ and the horizontal axis (where $\mathrm{Ha}=\mathrm{Ha}_1$), the critical wave number is $k=4.27$. The cells are almost spherical.

B. Required electric currents

Let I_{axis} be the axial current inside the inner cylinder and I_{fluid} the axial current through the fluid (i.e., between inner and outer cylinder). The toroidal field amplitudes at the inner and outer cylinders are then

$$B_{\mathrm{in}}=\frac{I_{\mathrm{axis}}}{5R_{\mathrm{in}}},\quad B_{\mathrm{out}}=\frac{(I_{\mathrm{axis}}+I_{\mathrm{fluid}})}{5R_{\mathrm{out}}}, \tag{24}$$

where R, B, and I are measured in cm, G, and A. Expressing I_{axis} and I_{fluid} in terms of our dimensionless parameters one finds

TABLE V. As in Table II, but for $\hat{\eta}=0.5$, and insulating boundaries.

$\hat{\mu}_B$	Ha_0	Ha_1	I_{axis} (kA)	I_{fluid} (kA)
−10	6.09	4.66	0.190 (0.599)	−3.99 (−12.6)
−5	11.8	9.31	0.380(1.20)	−4.18 (−13.2)
−4	14.6	11.7	0.477 (1.50)	−4.29 (−13.5)
−3	19.4	15.7	0.640 (2.02)	−4.48 (−14.1)
−2	29.3	25.2	1.03 (3.24)	−5.15 (−16.2)
−1	73.6	64.6	2.63 (8.31)	−7.89 (−24.9)
1	**∞**	**109.0**	**4.44 (14.0)**	**4.44 (14.0)**
2	∞	28.1	1.15 (3.61)	3.45 (10.8)
3	32.6	17.2	0.701 (2.21)	3.51 (11.1)
4	20.5	12.5	0.510 (1.61)	3.57 (11.3)
5	15.3	9.81	0.400 (1.26)	3.60 (11.3)
10	6.86	4.78	0.195 (0.615)	3.71 (11.7)

$$I_{\rm axis} = 5\ {\rm Ha}\frac{\hat{\eta}^{1/2}}{(1-\hat{\eta})^{1/2}}(\mu_0\rho\nu\eta)^{1/2} \tag{25}$$

and

$$I_{\rm fluid} = \frac{\hat{\mu}_B - \hat{\eta}}{\hat{\eta}} I_{\rm axis}, \tag{26}$$

in amperes. Note also how the required currents depend on the radius *ratio* $\hat{\eta}$, but not on the actual physical dimensions $R_{\rm in}$ and $R_{\rm out}$. Making the entire device bigger thus reduces the current *density*, inversely proportional to the square of the size. By making the device sufficiently large one can thereby prevent ohmic heating within the fluid from becoming excessive.

The results for the critical Hartmann numbers are now applied to two different conducting liquid metals, sodium and gallium-indium-tin [11], whose material parameters are given in Table I. We also wish to consider the effect of varying the radius ratio $\hat{\eta}$. Tables II and III give the values of the electric currents needed to reach the *lesser* of $\mathrm{Ha}^{(0)}$ and $\mathrm{Ha}^{(1)}$, for the two values $\hat{\eta}=0.25$ and 0.5, and for $\hat{\mu}_B$ ranging from -10 to 10 in each case. Note that for large $|\hat{\mu}_B|$, $\mathrm{Ha}^{(0)}$ scales as $1/\hat{\mu}_B$, and $I_{\rm fluid}$ approaches a constant value. The calculated currents are lower for fluids with smaller $\sqrt{\mu_0\rho\nu\eta}$ (i.e., sodium is better than gallium).

In these tables, the most interesting experiment, with the almost uniform field $\hat{\mu}_B=1$ (see Fig. 3, top right) is indicated in bold. For a container with a medium gap of $\hat{\eta}=0.5$, parallel currents along the axis and through the fluid of 6.16 kA for sodium and 19.4 kA for gallium are necessary. Such sodium experiments should indeed be possible. Experiments with a wider $\hat{\eta}=0.25$ gap are even easier; in that case even gallium experiments should be possible, with a current of 9.29 kA required (see Table II).

The Reynolds numbers that would be required to obtain not just these Re=0 pure Tayler instabilities, but also the transition points from $m=0$ to $m=1$ are also not difficult to achieve; for $R_{\rm out}\sim 10$ cm, say, rotation rates of order 10^{-2} Hz are already enough.

C. Insulating cylinder walls

Calculations were also done for insulating cylinder walls; the results are given in Figs. 6 and 7. They are generally similar to those for the conducting cylinders, but with one important exception. The $m=0$ and $m=1$ stability curves now almost always cross one another, as they do for conducting cylinders only for almost current-free B_ϕ profiles. For $\hat{\mu}_B\simeq 1$ profiles one can again observe how for weak fields the $m=0$ mode *stabilizes* the rotation until beyond the crossover point the $m=1$ mode strongly *destabilizes* the rotation.

V. CONCLUSIONS

We have shown how complex the interaction of magnetic fields and differential rotation can be in magnetohydrodynamic Taylor-Couette flows, including also a strong dependence on the magnetic Prandtl number. For large Pm the field destabilizes the differential rotation, whereas for small Pm it stabilizes it. However, if the field (or rather the current) is too great, then the Tayler instabilities will always destabilize any differential rotation.

In order to prepare laboratory experiments, we also did calculations at values of Pm appropriate for liquid metals, for both conducting and insulating cylinder walls. In particular, we considered the almost uniform field profile $\hat{\mu}_B=1$. For both conducting and insulating boundaries, the field is initially stabilizing, but after the most unstable mode switches from $m=0$ to $m=1$ it is strongly destabilizing, until the pure Tayler instability sets in even at Re=0.

For various gap widths and field profiles, we also computed the critical Hartmann numbers and the corresponding electric currents. Tables II–V give the required currents for both conducting and insulating walls; note how insulating walls (Tables IV and V) typically require lower currents than conducting walls (Tables II and III). The other clear trend is that the currents are smaller for wider gaps and larger for narrower gaps. An optimal experiment might therefore have $\hat{\eta}=0.25$, insulating walls, and $\hat{\mu}_B=1$, which would require only 6.84 kA even with gallium-indium-tin (Table IV).

ACKNOWLEDGMENTS

The work of D.S. was supported by the Helmholtz Institute for Supercomputational Physics in Potsdam and partly by the Leibniz Gemeinschaft under program SAW.

[1] S. Chandrasekhar, *Hydrodynamic and Hydromagnetic Stability* (Clarendon, Oxford, 1961).
[2] R. J. Donnelly and M. Ozima, Proc. R. Soc. London, Ser. A **226**, 272 (1962).
[3] R. J. Donnelly and D. R. Caldwell, J. Fluid Mech. **19**, 257 (1964).
[4] A. P. Willis and C. F. Barenghi, J. Fluid Mech. **463**, 361 (2002).
[5] E. P. Velikhov, Sov. Phys. JETP **9**, 995 (1959).
[6] S. A. Balbus and J. F. Hawley, Astrophys. J. **376**, 214 (1991).
[7] G. Rüdiger and Y. Zhang, Astron. Astrophys. **378**, 302 (2001).
[8] H. T. Ji, J. Goodman, and A. Kageyama, Mon. Not. R. Astron. Soc. **325**, L1 (2001).
[9] R. Hollerbach and G. Rüdiger, Phys. Rev. Lett. **95**, 124501 (2005).
[10] G. Rüdiger, R. Hollerbach, F. Stefani, T. Gundrum, G. Gerbeth, and R. Rosner, Astrophys. J. Lett. **649**, L145 (2006).
[11] F. Stefani, T. Gundrum, G. Gerbeth, G. Rüdiger, M. Schultz, J. Szklarski, and R. Hollerbach, Phys. Rev. Lett. **97**, 184502 (2006).

[12] F. Stefani, T. Gundrum, G. Gerbeth, G. Rüdiger, J. Szklarski and R. Hollerbach, New J. Phys. **9**, 295 (2007).
[13] Y. V. Vandakurov, Sov. Astron. **16**, 265 (1972).
[14] R. J. Tayler, Mon. Not. R. Astron. Soc. **161**, 365 (1973).
[15] N. A. Krivova and S. K. Solanki, Astron. Astrophys. **394**, 701 (2002).
[16] H. Korhonen, S. V. Berdyugina, K. G. Strassmeier, and I. Tuominen, Astron. Astrophys. **379**, L30 (2001).
[17] J. Braithwaite and Å. Nordlund, Astron. Astrophys. **450**, 1077 (2006).
[18] J. Braithwaite, Astron. Astrophys. **453**, 687 (2006).
[19] D. Michael, Mathematika **1**, 45 (1954).
[20] G. Rüdiger and D. Shalybkov, Phys. Rev. E **66**, 016307 (2002).
[21] P. A. Gilman and P. A. Fox, Astrophys. J. **484**, 439 (1997).